

Featuring work from Professor Pinar Zorlutuna's Laboratory, Department of Aerospace and Mechanical Engineering, University of Notre Dame, U.S.A.

A multiplexed ion-exchange membrane-based miRNA (MIX·miR) detection platform for rapid diagnosis of myocardial infarction

This work reports a multiplexed ion-exchange membrane-based miRNA sensor, namely MIX.miR, for detection of multiple specific cardiac-associated exosomal miRNA markers in clinical plasma samples from patients with stable coronary artery disease (CAD), ST-elevation myocardial infarction (STEMI) prior to (STEMI-pre) and following percutaneous coronary intervention (STEMI-PCI), and no evident coronary artery disease (NCAD) groups.

As featured in:



See Pinar Zorlutuna *et al.*,
Lab Chip, 2021, **21**, 3876.



Cite this: *Lab Chip*, 2021, **21**, 3876

A multiplexed ion-exchange membrane-based miRNA (MIX·miR) detection platform for rapid diagnosis of myocardial infarction†

Xiang Ren, Bradley W. Ellis,^a George Ronan,^a Stuart Ryan Blood,^b Cameron DeShettler,^b Satyajayoti Senapati,^b Keith L. March,^c Eileen Handberg,^c David Anderson,^c Carl Pepine,^c Hsueh-Chia Chang ^{ab} and Pinar Zorlutuna ^{*ab}

Micro RNAs (miRNAs) have shown great potential as rapid and discriminating biomarkers for acute myocardial infarction (AMI) diagnosis. We have developed a multiplexed ion-exchange membrane-based miRNA (MIX·miR) preconcentration/sensing amplification-free platform for quantifying in parallel a panel of miRNAs, including miR-1, miR-208b, and miR-499, from the same plasma samples from: 1) reference subjects with no evident coronary artery disease (NCAD); 2) subjects with stable coronary artery disease (CAD); and 3) subjects experiencing ST-elevation myocardial infarction (STEMI) prior to (STEMI-pre) and following (STEMI-PCI) percutaneous coronary intervention. The picomolar limit of detection from raw plasma and 3-decade dynamic range of MIX·miR permits detection of the miRNA panel in untreated samples from disease patients and its precise standard curve, provided by large 0.1 to 1 V signals and eliminates individual sensor calibration. The use of molecular concentration feature reduces the assay time to less than 30 minutes and increases the detection sensitivity by bringing all targets close to the sensors. miR-1 was low for NCAD patients but more than one order of magnitude above the normal value for all samples from three categories (CAD, STEMI-pre, and STEMI-PCI) of patients with CAD. In fact, miR-1 expression levels of stable CAD, STEMI-pre and STEMI-PCI are each more than 10-fold higher than the previous class, in that order, well above the 95% confidence level of MIX·miR. Its overexpression estimate is significantly higher than the PCR benchmark. This suggests that, in contrast to protein biomarkers of myocardial injury, miR-1 appears to differentiate ischemia from both reperfusion injury and non-AMI CAD patients. The battery-operated MIX·miR can be a portable and low-cost AMI diagnostic device, particularly useful in settings where cardiac catheterization is not readily available to determine the status of coronary reperfusion.

Received 2nd August 2021,
Accepted 13th September 2021

DOI: 10.1039/d1lc00685a
rsc.li/loc

Introduction

Acute myocardial infarction (AMI) is the primary cause of death among cardiovascular diseases.^{1,2} The diagnosis of AMI requires accurate analytical results from biomarkers in a timely manner. The current clinical standard of diagnosis combines echocardiogram (ECG) and several circulating protein biomarkers from plasma.^{3,4} Though ECG results can be obtained within minutes of presentation, biomarker

results typically take hours after blood sampling because of the various pretreatment and reverse-transcription PCR steps. These pretreatment steps also have low yield, thus compromising the sensitivity of the test. In their current state, both are incapable of distinguishing between patients with and without complete coronary occlusion, unless additional invasive testing is implemented, and both have significant false positive rates. These issues prolong diagnosis and treatment, contributing to increased mortality rates.^{3–6} New approaches for diagnosing AMI and the status of coronary occlusion remain an unmet clinical need. In particular, differentiation of ongoing ischemia in the absence of reperfusion from reperfusion injury has important treatment implications.

MicroRNAs (miRNAs) are small (17–22 nucleotides) non-coding RNAs that regulate gene expression at a posttranscriptional level by targeting messenger RNAs (mRNAs).⁷ miRNAs play a critical role in homeostasis, and

^a Department of Aerospace and Mechanical Engineering, University of Notre Dame, Notre Dame, IN 46556, USA. E-mail: pinar.zorlutuna.1@nd.edu;

Tel: +1 (574)631 8543

^b Department of Chemical and Biomolecular Engineering, University of Notre Dame, Notre Dame, IN 46556, USA

^c Division of Cardiology, Department of Medicine in the College of Medicine, University of Florida, Gainesville, FL 32611, USA

† Electronic supplementary information (ESI) available. See DOI: [10.1039/d1lc00685a](https://doi.org/10.1039/d1lc00685a)

their dysregulation has been associated with many disease states including AMI and coronary artery disease (CAD).⁸ Links have been made to miRNA profiles in diagnostic, prognostic, and even therapeutic roles.⁹ Circulating miRNAs have recently been proposed as potential biomarkers for rapid and accurate assessment of several diseases such as cancer, AMI, CAD, and other cardiovascular diseases.^{9–14} As miRNA turnover is much quicker than that of proteins, we hypothesized that assessment of miRNAs could be used to distinguish between AMI patients who have undergone reperfusion and those who have not, significantly decreasing the amount of testing needed prior to diagnosis. Recent pre-clinical studies have shown that several miRNAs, specifically miR-1, miR-208b, and miR-499, have the potential to accurately diagnose AMI.^{2,8,15–20} However, current methodology to detect changes in plasma miRNA levels relies on a series of procedures which render the process lengthy and quantitatively unreliable, so that profiling of miRNAs is impractical to guide therapy in the setting of AMI. Specifically, plasma contains many PCR inhibitors and hence the miRNAs are extracted with a low-yield (<10%) extraction kit.²¹ The yield of this extraction is further reduced by agents added to lyse the exosome carriers of the miRNAs.²² The conversion of 20–25 nucleotide miRNA to cDNA long enough for the primers involves a hairpin or toehold ligation step with a pairing sequence no longer than 10 bases. Such a short pairing sequence produces highly biased conversion that renders the quantification inaccurate. Extensive normalization is thus required for each miRNA, and it remains unclear whether such normalization would be valid for all samples. An accurate pretreatment and RT-PCR free profiling technology is hence needed for miRNA profiling to be a viable diagnostic platform.

Microfluidic preconcentration/sensing technologies have shown promise in replacing RT-qPCR as an alternative for miRNA profiling. Electrochemical impedance spectroscopy (EIS),^{23–28} for example, can yield highly accurate quantification. However, because of spurious reactions with other reagents in the plasma sample, the selectivity is often undesirable unless tedious blocking of the electrode with surfactant monolayers is carried out. A new type of electrokinetic sensor based on ion-exchange membranes (anion exchange membranes (AEM) for miRNA sensing) eliminates this selectivity issue with a highly charged membrane surface that reduces attractive hydrophobic interactions with fouling plasma proteins.^{29,30} In the presence of a strong microfluidic wash flow, only target miRNAs that hybridize with their complementary oligonucleotides functionalized to the membrane surface remain on the surface. Due to the ion-depleting action of the membrane on the side of the functionalized oligonucleotide, the conductivity near that surface membrane is 3 orders of magnitude lower than the bulk or within the charged membrane. The surface layer hence controls the voltage drop and the additional surface charge of the hybridized duplex can sensitively gate the ion current, producing a voltage

signal much larger than those from electrochemical sensors. Additional ion-depleting membrane modules around the sensor can push and concentrate the charged analyte into a band around the sensor, thus increasing the local analytic concentration by as much as 3 orders of magnitude.³¹ When combined with a surface acoustic wave (SAW) exosome lysing module that does not require the addition of diluting and contaminating lysing solutions, this membrane-based microfluidic platform has demonstrated high-sensitivity miRNA detection from plasma samples without pretreatment or PCR amplification.^{32–34} The same technology has been extended to low viral infectious disease detection that requires PCR amplification and to protein biomarker detection.^{32–34} The depletion membrane can also be used for high-yield isolation of the virus RNA from PCR inhibitors²¹ and nanoparticle reporters can be used for a sandwich assay of proteins.²⁹

One important issue concerning miRNA profiling is whether the miRNAs are exosomal. There is growing evidence that smaller nanocarriers like lipoproteins and ribonucleoproteins can also carry miRNAs, sometimes known as free-floating miRNAs. In our earlier studies, we have found evidence of miR21 in ribonucleoproteins⁴⁹ when plasma from cancer patients is not lysed to release the exosomal miRNAs. However, gold standard methods for exosome isolation like ultra-centrifugation and size-exclusion chromatography are time consuming and low yield. The SAW lysing module permits us to determine if the miRNAs are exosomal, as any incremental miRNAs after lysing must come from the exosomes. It allows us to decide if SAW lysing is necessary for the actual sample.

These early membrane platforms for miRNA quantify only one target and are hence sensitive to sample-to-sample variations because of the small volume used for the chip. The preconcentration module also has large variation in its concentration efficiency. Hence, miRNA profiling would be much more accurate if multiple miRNA targets from the same sample are concentrated into the same mm-sized band and quantified, with one of them serving as an invariant reference. This requires all the sensors to be placed at the same band to minimize analyte loss that would occur if the band is moved from sensor to sensor. We hence develop a sensor capillary bundle with three sensor heads, each with its own working and reference electrodes. With multiple sensors, an electronically automated platform must also be developed. Multiple miRNA profiling hence requires new microfluidic design and novel miniature instrumentation. Here we describe such a miRNA platform (MIX-miR: multiplexed ion-exchange membrane-based miRNA), developed by integrating three specific miRNA AEM sensors into a single capillary sensing unit and by combining this sensing capillary with membrane preconcentration and SAW lysing modules. We use this platform to detect a panel of 3-target miRNAs within clinical samples derived from 4 categories of clinical samples.

We investigated three candidate miRNAs closely associated with AMI (miR-1, miR-208b, and miR-499) from clinical plasma samples of 1) reference subjects with no evident coronary artery disease (NCAD); 2) subjects with stable coronary artery disease (CAD); and 3) subjects experiencing ST-elevation myocardial infarction (STEMI) prior to (STEMI-pre) and following percutaneous coronary intervention (STEMI-PCI). Additionally, we tested all samples with and without the integrated SAW lysis device to confirm whether the measured miRNA was free-floating or inside extracellular vesicles. We then compared our measurements to the current gold standard detection of miRNA RT-qPCR measurements of the same samples. The data from the diseased samples from this study match well with current literature for the miRNAs tested. In addition, for the first time, this data demonstrates the ability to distinguish between STEMI patients that have undergone clinical intervention resulting in reperfusion from those that have not, for each of miR-1 and miR-208b, which suggests that these markers can discern ongoing ischemia from reperfusion injury. This study demonstrates the potential of the MIX·miR method as a low-cost point-of-care AMI diagnostic device providing results for multiple biomarkers in a more accurate and timely manner than current biomarker detection methods. This, along with its portability also makes the MIX·miR sensing platform a more viable AMI diagnostic tool in developing countries. Additionally, the MIX·miR can be utilized as a general miRNA quantification method that requires less sample preparation, is more accurate, and provides more rapid results than the current standard miRNA RT-qPCR.

Materials and methods

Ethics statement

The protocol was approved by University of Florida IRB (IRB#201901232). Written informed consent was obtained from all subjects and conformed to the Declaration of Helsinki.

Sample collection and preparation

Blood was collected *via* standard venous puncture from healthy subjects, subjects diagnosed with CAD, and patients diagnosed with STEMI with an observed obstruction (STEMI-pre) and following reperfusion (STEMI-PCI) (6 patients for all sample groups) into tubes containing ethylenediaminetetraacetic acid (EDTA). After collection, plasma was isolated by centrifuging at $1000 \times g$ for 5 min and the plasma was transferred to RNA free tubes and stored at -80°C and shipped to the University of Notre Dame. Once the clinical samples arrived at Notre Dame, they were thawed on ice, aliquoted and stored at -80°C until testing with the MIX·miR sensors.

Oligoprobes and calibration miRNAs

The oligoprobes and calibration miRNAs are purchased from Integrated DNA Technologies, Inc. The oligoprobes are: miR-1-1-complement ($5'$/5AmMC12/ATA CAT ACT TCT TTA CAT TCC A-3'$, MW = $6866.7 \text{ g mol}^{-1}$), miR-208b-complement ($5'$/5AmMC12/ACA AAC CTT TTG TTG GTC TTA T-3'$, MW = $6913.7 \text{ g mol}^{-1}$), and miR-499-5p-complement ($5'$/5AmMC12/AAA CAT CAC TGC AAG TCT TAA-3'$, MW = $6645.6 \text{ g mol}^{-1}$). The miRNA for calibration purposes are: miR-1-1 ($5'$/TGG AAT GTA AAG AAG TAT GTA T-3'$, MW = $6861.5 \text{ g mol}^{-1}$), miR-208b ($5'$/ATA AGA CGA ACA AAA GGT TTG T-3'$, MW = $6815.5 \text{ g mol}^{-1}$), and miR-499-5p ($5'$/TTA AGA CTT GCA GTG ATG TTT-3'$, MW = $6466.3 \text{ g mol}^{-1}$). All oligoprobes and calibration miRNAs were aliquoted and stored at -20°C .

miRNA isolation for RT-qPCR

miRNA was isolated from human plasma using the Maxwell RSC instrument (Promega, Wisconsin, USA) and miRNA plasma or serum miRNA isolation kit (Promega) with lysing solution and RNA paramagnetic bead cartridge extraction, as per the provided miRNA isolation protocol. Following miRNA isolation, samples were spiked with miRNA ath-miR-159a (Integrated DNA Technologies, Coralville, IA) at a concentration of 20 nM. cDNA was synthesized from the isolated miRNA for each specific miRNA that was to be tested (miR-1, miR-208b, miR-499, and ath-miR-159a; Thermo Fisher Scientific, Massachusetts, USA) using the custom Taqman reverse transcription for each miRNA following the provided Taqman custom reverse transcription protocol (Thermo Fisher). Preamplification was performed using Taqman Preamp Mastermix (Thermo Fisher) and custom miRNA assays for each miRNA tested (miR-1, miR-208b, miR-499, and ath-miR-159a; Thermo Fisher) following the provided Taqman custom preamplification protocol for 16 cycles. miRNA RT-qPCR was performed using the Taqman custom miRNA assays for each specific miRNA tested (miR-1, miR-208b, miR-499, and ath-miR-159a; Thermo Fisher) following the provided protocol. For data analysis the delta-delta CT method was utilized using the spiked in ath-miR-159a as the housekeeping miRNA.

miRNA isolation efficiency assay for RT-qPCR

A known mass (0.05 pg, 5 pg, and 500 pg) of ath-miR-159a was spiked into 300 μL of RNase free water at three different concentrations. miRNA was then isolated from the samples using the Qiagen miRNeasy kit (Qiagen, Germany) following the protocol as per manufacturer instructions. Following isolation, an additional clean up step was performed by running the miRNA solution through a 3KDa filtration column (Sigma Aldrich, Missouri, USA) at 14 000 g for 90 min and extracting the purified miRNA, after which the volume was normalized to 25 μL . The same 3 amounts of ath-miR-159a was also spiked into 25 μL of RNase free water as control. miRNA PCR was then performed as described above and expression of the isolated samples was

normalized to the spiked in samples that did not undergo miRNA isolation.

Experimental

Integration board

Fluidic device fabrication utilized previously established procedures.^{32,34} The principle of single AEM sensing miRNA is discussed in previous publications.^{30,35} The sensing capillary with 3 AEM sensors for 3 different miRNAs is similar to our earlier design for 4 serotypes of dengue RNA.³⁶ The AEM contains nanoporous (<1 nm) ion-selective granules in the membrane, which allows ion depletion across the membrane with an onset voltage. As illustrated in Fig. 1(d and e), the miRNAs will bond with the specific oligoprobes. Here we target miR-1, miR-208b, and miR-499 to study the clinical MI samples. Once the miRNAs attach to the AEM, the CVC (current–voltage curve) of the AEM will generate a larger voltage shift compared to the baseline of only oligoprobes on AEM. Briefly, the samples were thawed on ice and a volume of 20 μL was lysed by SAW. The SAW will break the extracellular vesicles, releasing their miRNAs into the sample. The sample is then flowed through the sensing channel of the MIX-miR sensor by a syringe pump at a constant flow rate of 250 $\mu\text{L h}^{-1}$. The flow channel is made of polycarbonate to reduce possible miRNA attraction with polydimethylsiloxane (PDMS). The AEM-based sensor itself is made of polyurethane for the same reason. The dimension of the flow channel is 45 mm in length, 300 μm in height, and

2 mm in width. An additional 200 mL of 1 \times phosphate-buffered saline (PBS) was used as driving fluid for the sensing channel. A pre-concentration unit, with two additional cation-exchange membranes (CEM), was activated with a constant current of 8×10^{-4} A to keep the miRNAs near the MIX-miR sensor for 20 min.^{30,35} The pre-concentration unit is connected to the fluidic channel *via* a pair of cation-exchange membranes (CEM). Both the AEM and CEM belong to the family of ion-exchange membranes (IEM) and allow only counter ions to pass through them. After several washes with PBS, the CVC of the sensor was measured in 0.1 \times PBS by a potentiostat connected to our integration board. The probe selection switches on the board can manually select each pair of electrodes for the potentiostat.

The integration board contains a binary coding and decoding circuit to control the selection of each miRNA target. The SAW lysing device can break down exosomes in the plasma samples to release miRNAs. The SAW device was built on a piezoelectric substrate with interdigitated electrodes.³¹ The sinusoid signal for generating the SAW is 28.16 MHz with 190 mV Vpp (peak to peak voltage, Agilent 33250A, Agilent Technologies, Inc, Loveland, CO). The signal was amplified to a power of 1 W *via* a RF power amplifier (Electronics & Innovation 325LA RF, Rochester, NY). To maintain the integrity of the miRNAs, we placed ice chips around the SAW device and sample inlet tubing. The SAW lysing device was washed with isopropanol (IPA) and deionized (DI) water after each usage.

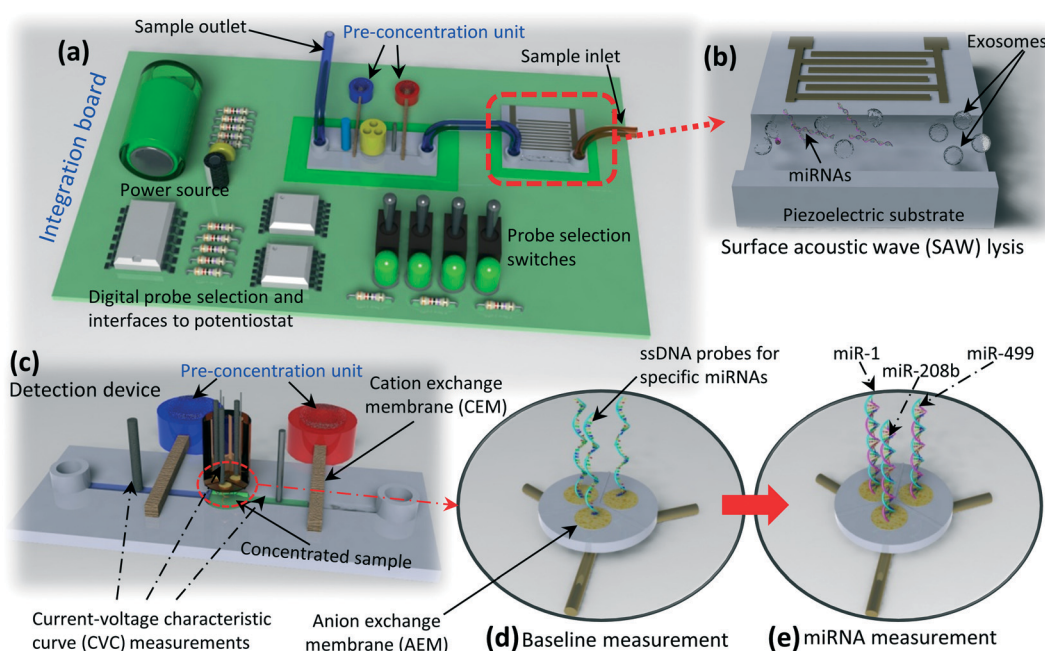


Fig. 1 Illustration of the integrated measurement of miRNAs using 3-membrane sensor. (a) The integration board with the detection device, the SAW lysing device, and the digital controlling (illustrative figure); (b) the SAW lysing device that breaks exosomes and releases miRNAs; (c) the detection device with the MIX-miR sensors, pre-concentration unit, and the electrodes connected to the potentiostat for CVC measurements; (d) the baseline measurement with 3 kinds of different ssDNA probes; (e) the measurements of miR-1, miR-208b, and miR-499.

MIX-miR sensor

The MIX-miR sensor was prepared by polyurethane (PU) molding with AEM embedded on the surface. The raw molds for the AEM sensor are printed by a 3D wax printer (Solidscape Studio, Merrimack, NH) with building wax as a sacrificial material. The molds for PU are made by mixing TAP silicone and catalyst (TAP Plastic, Seattle, WA) at a weight ratio of 10:1. The silicone mixture was casted on the wax mold. The wax mold is later dissolved in dimethyl sulfoxide (DMSO) followed by deep rinsing with IPA. The replica molding of TAP silicone was done following the PDMS casting methods using 3D wax printed molds to enhance the consistency of the MIX-miR sensors. The PU is solidified from the mixture of a two-component PU casting resin (TAP Plastic, Seattle, WA) at a weight ratio of 1:1. To covalently link the miRNA probes to the 3 AEMs, 20 μ L of 60 μ g μ L $^{-1}$ 3,3',4,4'-benzophenonetetracarboxylic acid (BPDA) was added

to the AEM surface and exposed to UV light for 90 s. After the carboxylation procedures (modifying the AEM surface with -COOH groups), three different miRNA probes complementary to miR-1, miR-208b, and miR-499 (Integrated DNA Technologies, Inc., Skokie, IL) were attached on each AEM using EDC/NHS coupling chemistry and incubated at 4 °C for 8 hours. Due to the presence of the additional Y-shaped barrier, the three different miRNAs cannot merge with each other, resulting in the functionalization of one probe to one AEM without any cross contamination. The baselines of the miRNA probes were measured first. The device went through a high ionic wash with 4 \times PBS to remove any miRNA complement and followed by a low ionic wash with 0.1 \times PBS to remove any high ionic residual. As illustrated in Fig. 2(e), the baselines for the 3 membranes showed linear regions, saturation regions, and over-limiting regions. As demonstrated in Fig. 2(g), only the miRNA complements attached to the AEM. The sample either with or

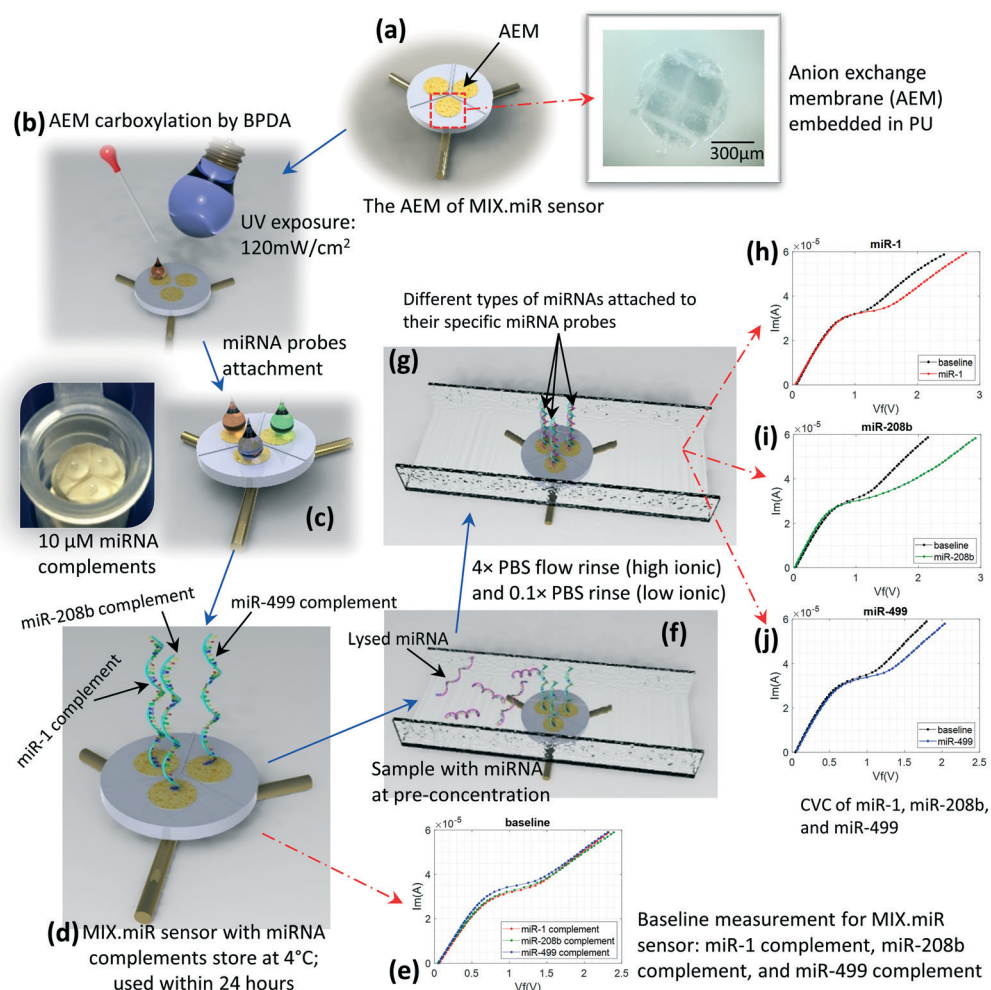


Fig. 2 The functionalization of the 3-membrane sensor with miR-1, miR-208b, and miR-499 and the CVC measurement procedure of each specific miRNA. (a) The illustration and the picture of the AEM embedded in the MIX-miR sensor; (b) AEM carboxylation step using BPDA; (c) miRNA complements attachment onto the AEM surfaces; (d) the MIX-miR sensor with three different kinds of miRNA complements; (e) the baseline measurement for MIX-miR sensor with only the miRNA complements; (f) miRNA sample during pre-concentration step; (g) high ionic wash and low ionic wash steps to remove non-specific miRNAs; (h–j) the CVC curve of miR-1, miR-208b, and miR-499, respectively.

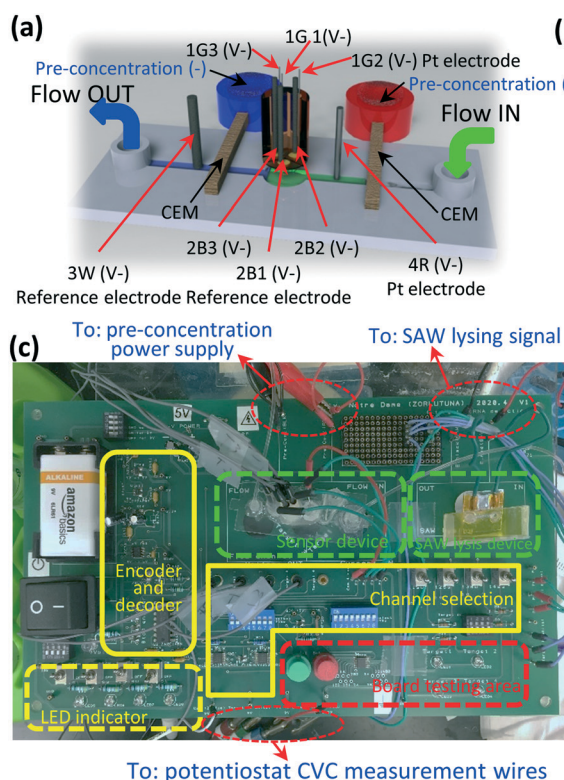
without SAW lysing was pumped into the fluidic device during pre-concentration. The miRNAs were able to attach to their specific miRNA probes. After another high ionic wash with $4\times$ PBS, the remaining miRNAs statically adhering to the AEM were removed. Finally, multiple low ionic washes with $0.1\times$ PBS were performed leaving only the targeted miRNAs covalently bonded to their specific oligoprobes. The CVC showed a voltage shift at the over-limiting region with twice the current in the saturation region.

Due to the depletion action by the AEM sensor and by an ensuing electroconvective instability,³⁰ the CVC curve is nonlinear, with a linear ohmic region, a saturated limiting-current region and a second linear overlimiting region with increasing voltage. The limiting current region results from the depletion action on the membrane surface, which increases the system resistance, and the overlimiting region is because ions are replenished into this depletion region by the electroconvective instability.³⁷ As shown in Fig. 2(e), the baseline measurements of the three different membranes are almost overlapping in the linear regions and the overlimiting regions. Our manufacturing method hence displayed promising consistency between the different AEM sensors. From the measurement of miR-1 (red dots curve), miR-208b (green dots curve), and miR-499 (blue dots curve), the voltage shifts in the over-limiting regions compared with the baselines (black dots curves in all three charts) are indicating

the different concentrations of each specific miRNA in the sample.

Experimental setup

The CVC is measured by the potentiostat with 4 electrodes: 2 platinum electrodes providing current input, and 2 reference electrodes collecting the voltage across the AEM. After the miRNAs hybridized with the miRNA probes, the CVC will show an increase of the voltage at the over-limiting region of the AEM, at the same current, due to the enhancement of the electroconvective instability that replenishes ions into the depleted region near the membrane. As illustrated in Fig. 3(a), the sensing electrodes are assigned with the color codes consistent with the wire color of the potentiostat (Gamry Reference 600, Gamry Instruments, PA). The electrodes 1G (green) and 4R (red) are applying current across the AEM, while 2B (blue) and 3W (white) are measuring the voltage across the AEM. The current applying on 1G and 4R is $0\text{--}8 \times 10^{-5}\text{ A}$, with a scanning step of $1 \mu\text{A s}^{-1}$. Here the three membrane chambers are sharing the common 3W and 4R. The pre-concentration unit is used to keep the negatively charged miRNAs in the sample near the AEM sensors with oligoprobes. The pre-concentration units are made by two pieces of CEM connecting the main flow channel with the pre-concentration reservoirs. The reservoirs are filled with



I/O Code	Binary coding and the assignments of electrodes			
	1G (I+)	2B (V+)	3W (V-)	4R (I-)
a ₁ a ₀ =00	1G1	2B1	com	com
a ₁ a ₀ =01	1G2	2B2	com	com
a ₁ a ₀ =10	1G3	2B3	com	com
a ₁ a ₀ =11	NC	NC	NC	NC

I/O: input/output; G: green; B: blue; W: white; R: Red; com: common port; NC: not connected.

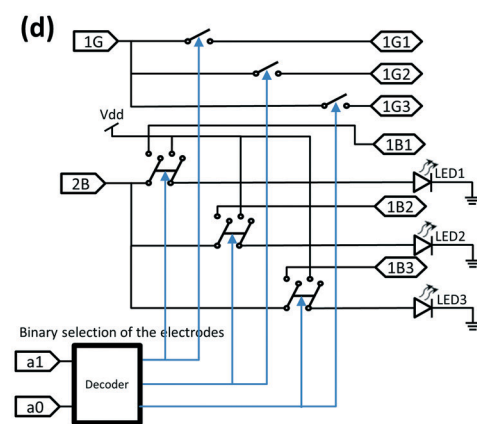
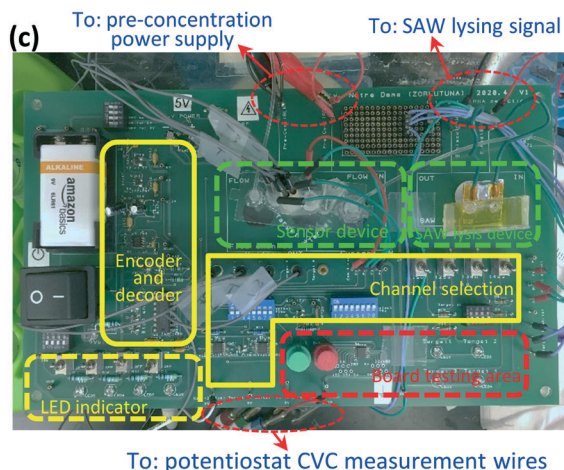


Fig. 3 Experimental setup: (a) the electrode assignment in the CVC measurements; (b) the binary code selection of the electrodes for potentiostat wires: #1 green, #2 blue, #3 white, and #4 red; (c) the integration board with fluidic devices and SAW lysing modulus during measurements; (d) binary coding selection of different miRNAs with LED indication.

10× TAE buffer to enhance conductance along the channel. Two platinum wires are placed in the pre-concentration reservoirs and connected to a power source (Keithley Instruments, Cleveland, OH) with a constant current of 8×10^{-4} A. The maximum voltage applied on the pre-concentration reservoirs is 200 V to avoid possible damage to the CEM. The pre-concentration is performed for 20 min during the sample flow. Since the miRNAs are negatively charged, the positive side of the pre-concentration unit attracts the miRNAs towards the positive side, which is the opposite direction of the sample flow. When the force from the pre-concentration and the flow are balanced, the miRNAs will stay near the AEM oligoprobes.^{30,35} Once the pre-concentration procedure finishes, the 10× TAE buffer in the reservoirs is replaced by 0.1× PBS to avoid interference with the potentiostat measurements. Multiple high ionic washes and low ionic washes are made through the sensing channel prior to the miRNA measurements.

Fig. 3(c) depicts the MIX-miR board prototype that can detect up to 3 different types of miRNAs. The SAW lysis device was activated to lyse exosomes and release the enclosed miRNAs into the sample. The flow inlet allows the exosomal miRNA to travel through the pre-concentration unit and concentrate at the sensing area at the center of the flow channel. The sensing reservoir is separated into 3 individual compartments. Each compartment has one functionalized AEM with a specific oligoprobe for each type of miRNA. Each compartment is connected to one pair of sensing electrodes. During the experiment, we use the selection switch on the board to select the correlated miRNA, instead of unplugging the sensing electrode from the reservoir for the following reasons. First, the plugging and unplugging of the sensing electrodes may introduce bubbles into the reservoir, which will cause CVC measurement error. Second, repeated use of the sensing electrodes requires multiple calibration steps before each measurement. By using this board, we only need to perform one calibration in advance and keep the sensing unit running during the CVC measurement. Finally, this also avoids possible contamination between different compartments.

The integration board was designed using commercial software PCBArtist® and fabricated by the PCB manufacturer (Advanced Circuits, Aurora, CO) linked with the software (detailed layout is described in ESI†). On this board, we have a green light-emitting diode (LED) for the indication of power supply, and four individual LED to indicate each miRNA target 1, 2, 3, and 4, respectively. The selection function is achieved by the encoder and decoder. The multiplexer is used to selectively connect each pair of sensing electrodes to the signal interface with the potentiostat equipment. The 9 V battery and voltage regulators on the board allow for the possibility of having the board run without the presence of an external power supply. This also indicates that our self-designed board has the ability to be further miniaturized to a hand-held device for point-of-care miRNA sensing. This prototype board utilizes economic electronic parts with the

total cost for one board being approximately \$55 (\$33 for the PCB, \$22 for the electronic parts, battery included). Other than the encoder, the board also contains buffers and filters to reduce electronic noise. In addition, to avoid the possible noise generated from the wiring and regulators, the layout of the board is optimized with large ground lines and non-crossing and interference signal lines. The electronic testing of the connection shows that the wiring and connection resistance between each pair of electrodes are less than 5 Ω, which is significantly less than the impedance of the sensing IEM with or without miRNA.

This MIX-miR board is not a simple switch board. The binary coding in Fig. 3(d) provides an example of effective controlling of the multiple-target miRNA sensing. We used two stages of the selection device to control the two parallel circuits for both the platinum electrodes (1G and 4R) and the reference electrodes (2B and 3W), as well as the LED indicators. We can use 2 bits to control up to 4 different targets. If we want to expand the size of the miRNA panel, we can increase the bit number to effectively select each targets. For instance, 3 bits ($a_2a_1a_0$) can control 8 different miRNA targets; 4 bits ($a_3a_2a_1a_0$) can control 16 different miRNA targets, etc. The binary digital controlling can allow us to expand the scale of this miRNA sensing to ultra-high-throughput detection of multiple different miRNA targets simultaneously.

Results

The CVC voltage shifts were correlated with miRNA concentration through calibration curves as shown in Fig. 4. We prepared the standard concentration of 0.1 pM, 1 pM, 10 pM, 100 pM, 1 nM, and 10 nM of each miRNA. The CVC voltage shifts were obtained by pre-concentration of 20 μL of each sample after a high ionic wash with 4× PBS and multiple low ionic washes with 0.1× PBS. The accuracy of MIX-miR sensors were also tested by comparing the standard concentration miRNA of 100 pM with the calibration curves.

The results of the calibration curves indicate a linear increase of the CVC voltage shifts on each decade of the concentration increments. This is consistent with our earlier theories that the charged molecules change the effective surface potential that drives the electroconvective instability. The voltage shifts observed across the AEM after miRNA attachment were studied using the Langmuir adsorption model.^{31,38} The correlations in the linear region of the Langmuir isotherm are described by

$$\frac{V}{RT/F} = A \log_{10} \left(\frac{C}{C_r} \right)$$

with A and reference concentration C_r being (4.70, 0.0104), (7.11, 0.0651) and (8.41, 0.0786) for the three miRNAs, respectively. The coefficient A is close to the theoretical value of $2 \ln(10)$ by Sensale *et al.*³⁷ The constants are Faraday's constant $F = 9.648 \times 10^4$ C mol⁻¹; Boltzmann constant $R =$

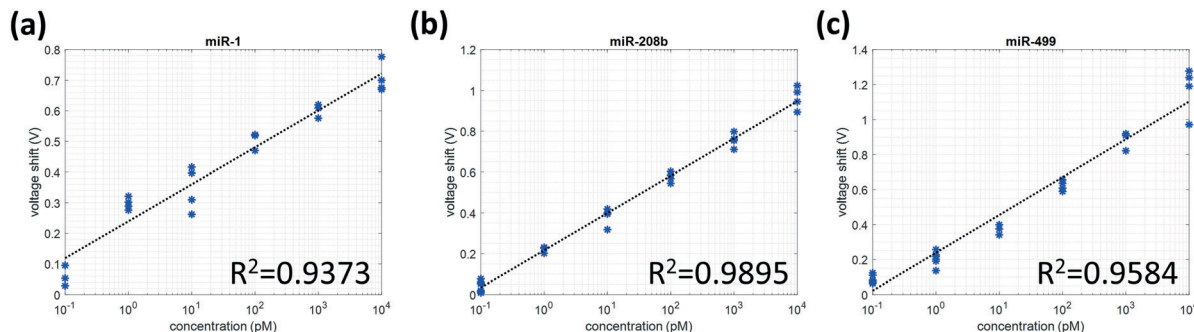


Fig. 4 The calibration curves of (a) miR-1, (b) miR-208b, and (c) miR-499 using the standard concentration of 0.1 pM, 1 pM, 10 pM, 100 pM, 1 nM, and 10 nM.

8.314 J ($\text{mol}^{-1}\cdot\text{K}^{-1}$); and room temperature $T \approx 25^\circ\text{C} = 298\text{ K}$. These correlations are valid between the limit of detection of pM and nM with R values indicated in Fig. 4. They correspond to roughly a maximum error in the concentration estimate by a factor of 1.04, 0.438, and 0.865 for miR-1, miR-208b, and miR-499, respectively. The linear fitting of the calibration curve can accurately correlate the measured miRNA from clinical samples within the concentration range of 0.1 pM to 10 nM. We hence prefer to work above 0.1 pM, the limit of detection (LOD).

The clinical samples from subjects in the NCAD, CAD, STEMI-pre, and STEMI-PCI groups were measured

individually. The results from each bar graph are repeated with six different independent patient samples. Since the calibration curves of the MIX-miR sensors are testing the miRNA concentrations between 0.1 pM and 10 nM, we diluted the STEMI-PCI samples by 5 times in 1× PBS. The concentrations of the 3 miRNAs in STEMI-PCI samples (purple bar graph) in Fig. 5(b) are readings after correction for the dilution factor. The error bars represent 95% confidence levels. The uncertainty of each group is defined by $u = t_{n-1,0.95}\sigma/\sqrt{n}$, where $n - 1$ is the freedom. From the measurement results in Fig. 5(b) with SAW lysing and those in Fig. 5(d) without SAW lysis, it is quite clear that the

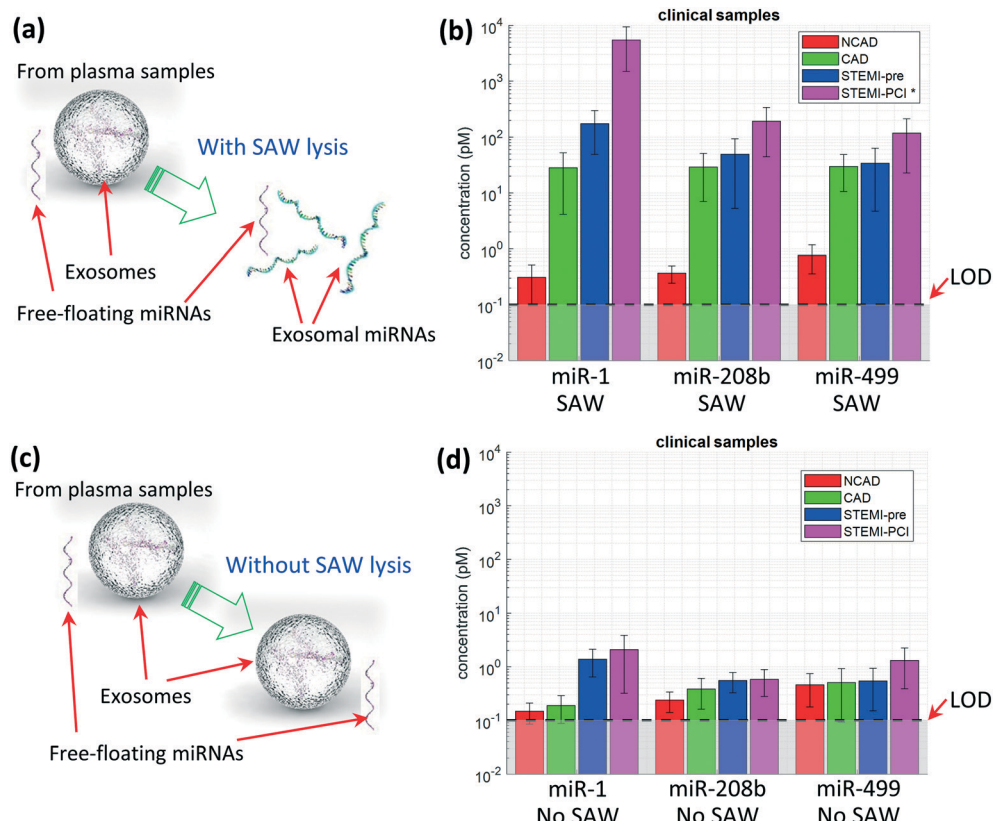


Fig. 5 The concentration of the miR-1, miR-208b, and miR-499 in clinical samples: (a & b) with SAW lysis; and (c & d) without SAW lysis. The error bars in (b) and (d) represent the 95% confidence level. LOD indicates the detection limit of the MIX-miR sensors (*: the STEMI-PCI sample with SAW lysis is diluted by 5 times in 1× PBS. The results of purple bar graphs with SAW lysing are multiplied by 5 after gaining the concentrations).

candidate miRNAs are exosomal and are only detectable after SAW lysis releases them from the nanocarrier exosomes. The MIX-miR sensor measurements in Fig. 5(d) indicate a low concentration around or less than 10 pM for all three different miRNAs. The miRNA concentrations below 0.1 pM are below the detection limit of the MIX-miR sensor.

For the SAW lysed samples, the MIX-miR measurements revealed that the cardiac-associated miRNAs, miR-1, miR-208b, and miR-499, were elevated in CAD as well as in STEMI subjects, both pre- and post-clinical intervention. The NCAD sample provided us with a baseline measurement of the miRNAs. The three candidate miRNAs yield signals near the pM LOD and hence cannot be reliably detected even after SAW lysis (miR-1: 0.31 ± 0.21 pM, miR-208b: 0.37 ± 0.12 pM, miR-499: 0.77 ± 0.41 pM). The samples from all patients with CAD showed a dramatic 10–100-fold increase in all three miRNAs (miR-1: $p = 0.01$, miR-208b: $p = 0.004$, miR-499: $p = 0.002$). The STEMI-pre samples revealed a >10-fold higher expression of miR-1 than the CAD samples, and roughly the same order of expression for miR-208 and miR-499 with miR-1 ($p = 0.03$), miR-208b ($p = 0.3$) and miR-499 ($p = 0.7$). This is in agreement with current literature, which has shown that the elevation of miR-499 in AMI patient plasma is often below the detection limits of conventional miRNA quantification methods due to irregular expression.^{16,39,40} There are reports with miR-1 and miR-208b being overexpressed up to 1000 times compared to normal samples.^{41–44} Comparing the STEMI-pre and STEMI-PCI, the STEMI-PCI samples demonstrated an additional increase in miR-1 and miR-208b, with miR-1 being overexpressed by another >10-fold increase (miR-1: $p < 0.001$, miR-208b: $p = 0.06$, miR-499: $p = 0.07$). Consequently, miR-1 varies significantly among CAD, STEMI-pre and STEMI-PCI samples. This finding suggests that miR-1 is a good biomarker that can differentiate between ischemia and reperfusion injury, in addition to distinguishing STEMI patients from CAD patients. miR-208b can differentiate STEMI and CAD patients from NCAD samples. However, the candidate miR-499 is involved in more complicated dynamics during AMI, which regulates the mitochondrial behaviors and affects the severity of the AMI.⁴⁵ Its relative invariance among the three groups of CAD subjects would suggest that it may be a reasonable reference control for plasma samples from patients with suspected cardiac disease.

We also conducted PCR quantification of three miRNAs in the clinical samples. Only miR-1 was detectable with the PCR tests. The other two miRNAs, miR-208b and miR-499, are not detectable in the same clinical samples after several attempts (data not shown). This is likely due to loss of miRNAs during sample preparation for PCR. To evaluate the loss of miRNA during the isolation step that is necessary to perform PCR, the efficiency of miRNA isolation was measured. Efficiency was observed to be much higher (~88%) at high concentrations of miRNA (1.6 μ M) whereas at lower concentrations (16 nM and 160 pM), like the ones we had for miR-208b and miR-499, efficiency dropped to below 50% and

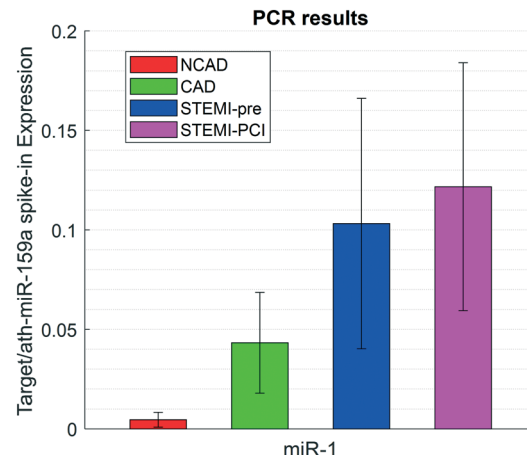


Fig. 6 miR-1 PCR results of clinical samples: NCAD, CAD, STEMI-pre, and STEMI-PCI. The error bars represent one standard deviation.

40%, respectively (ESI† Fig. S2). The PCR results in Fig. 6 indicate a significant increase in miR-1 expression in all samples when compared to NCAD. The relative overexpression level is qualitatively similar but quantitatively different from earlier miRNA RT-qPCR results in the literature.^{2,42,46–48} According to our results in miRNA isolation efficiency, the lower concentrations of miRNA have a higher loss ratio than the high concentrations of miRNA in PCR. The quantitative results of miR-1 by PCR are not fully representing the amount of miR-1 in each sample. There is also qualitative agreement with the SAW lysed MIX-miR data in Fig. 5(b). However, the MIX-miR overexpression level is orders of magnitude higher, with smaller error bars. The PCR results are, however, quantitatively comparable to the MIX-miR data without SAW lysing.

Discussion

The most striking of our MIX-miR results is the orders of magnitude discrepancy in expression of miR-1, and the difference in the ability to detect miR-208b and miR-499 when comparing Fig. 5 to the RT-PCR benchmark in Fig. 6. Since the PCR quantification of miR-1 was comparable to the non-lysed MIX-miR data, the majority of the miRNAs is lost due to inefficiency in miRNA extraction. This yield is expected to be even lower with chemical lysing. There are several other steps that can lead to significant RNA quantification errors. A small fraction of the extract is used in the PCR tube due to capacitance issues. Literature indicates that the extraction yield can be less than 10%,²¹ although careful benchmarking of trizol/phenol/chloroform, silica column and paramagnetic bead extraction has not been done. From our own experiments for this study, the efficiency of miRNA isolation for PCR provided an estimated loss of >60% in the samples with miRNA concentrations of 160 pM or less. Careful estimates of the miRNA reverse-transcription yield are also not available in literature. The duplication of short length miRNA (~22 nucleotides) may cause errors due

to the heterogeneity of the exosomal miRNA mixtures and by the necessary ligation step, despite the normalization effort. Analyte loss from PCR assays due to inefficient exosome lysing, RNA extraction and reverse transcription can reduce the miRNA copy number by several orders of magnitude, severely corrupting the assay sensitivity and quantification accuracy even if PCR itself has a limit of detection of several copies. Without the need for the additional sample preparation such as miRNA isolation and reverse-transcription steps in PCR and with SAW lysing and significant reduction in sample preparation and assay time (<1-hour *vs.* ~8 hours for RT-PCR), the MIX·miR sensor can hence provide a much faster assay for more biomarkers and with far higher sensitivity.

The AEM-based miRNA detection by electrical properties using fluidic devices demonstrates a potentially more efficient and accurate method for biological analysis. With the presence of a current across the IEM, either AEM or CEM, the *trans* and *cis* sides will become one depletion side and another enrichment side according to the concentration polarization theory. The voltage difference between the two sides will become linear with current again after reaching the overlimiting region, caused by electroconvection, water splitting, exaltation, and ion selectivity variations.³⁰ Our previous work has demonstrated our ability to manipulate this phenomenon for single miRNA target detection for cancer diagnosis. Chang *et al.* have reported single miRNA detection of miR-146a for oral cancer,³⁴ miR-21 for liver cancer,⁴⁹ and miR-550 for pancreatic cancer³¹ with the AEM sensor. However, for many biological diagnostics, multiple kinds of miRNA targets need to be considered concurrently. In the diagnosis of AMI or CAD, a single biomarker is not necessarily sufficient as a label for differentiating specific diseases.^{3–5,7} Moreover, some evidence suggests that single miRNA biomarkers sometime fail to correlate with current clinical biomarker analysis.^{16,47} In addition, concurrent detection of multiple targets from the same sample can reduce the possible variations inherent in biological samples. Since the miRNAs are also sensitive to temperature once released from exosomes, detecting more miRNAs within a shorter time can also reduce the error.^{15,50} Furthermore, testing multiple biomarkers on a single assay would decrease the time from admission to AMI diagnosis and treatment when compared to traditional protein biomarker testing, which must be done with separate assays, increasing patient survivability.^{3–5} With both the multiplexing aspect of the MIX·miR and the integration board, we are able to select different chambers for specific miRNA measurements. The digital control on the board provides us the potential to further increase the parallel quantity to enhance the multiple-target sensing ability.

Recent studies have suggested miRNAs as more appropriate biomarkers for the diagnosis of AMI due to early observations of rapid changes in their expression, and have identified that miR-1, miR-208b, and miR-499 were among the most viable candidates for clinical use.^{2,8,16–20} miR-1 is

associated with the early stage of AMI that is related to the cardiac conductance; while miR-208b and miR-499 are associated with the late stages that regulate the expression of sarcomere contractile proteins.^{51–53} Studies utilizing clinical samples suggest that miR-1 is a promising prospective biomarker for the early diagnosis of AMI to differentiate from other cardiovascular diseases.^{2,16,18–20,54} miR-208b has also been demonstrated to show a discernible increase during AMI.^{2,17,18} However, its onset is often more delayed in AMI pathogenesis than miR-1, with detection not occurring until approximately one hour following symptom onset.⁵⁵ Extensive clinical evidence suggests that similar to miR-1, miR-208b has a good correlation with the troponin assay.^{16,47,56} miR-499 is another cardiac associated marker that is detectable in AMI,^{18–20} though its elevation during disease progression is not as prominent as seen for miR-1 and miR-208b, making this increase more difficult to observe using traditional miRNA detection techniques.⁴⁰ Traditional methods in quantifying miRNA by RT-qPCR have trouble detecting miRNA at low concentrations due to the low efficiency of extraction during miRNA isolation and requires extensive sample preparation and processing work in miRNA isolation and amplification when compared to the MIX·miR, increasing potential error.^{21,22,31,33,34,49} Additionally, SAW lysis allows for the rapid (~1 min) mechanical lysis of exosomes without additional sample preparation. SAW lysing of exosomes to release exosomal miRNA without upstream exosome isolation only makes sense if the exosomal miRNA is much more abundant than their free-floating counterparts. This is clearly evident in Fig. 5. This method is hence more efficient and simpler than chemical lysing which involves additional chemical procedures and sample preparation steps. It also eliminates the need for a tedious exosome isolation step.

Unlike other miRNA detection methods such as RT-qPCR, the MIX·miR sensor does not require upstream sample preparation, *i.e.* the miRNA isolation, reverse transcription, and potential preamplification required for miRNA PCR, so that measurements may be made directly from plasma obtained within minutes of sampling. In addition, the same sample can be used to measure either free floating or free floating and exosomal miRNA through the use of SAW, something that would require additional samples and sample preparation with other miRNA detection methods.⁵⁷ The SAW lysis method utilizes a non-contact methodology to break the exosomes to release the exosomal miRNA with no additional chemicals. Additionally, the time from sample input to readout in the MIX·miR sensor is less than 30 minutes, significantly shorter than the thermocycling time needed for RT-qPCR. The sample volume required by the MIX·miR detection is only 20 µL; however, reliable PCR experiment requires 300–500 µL of the sample. Without the need for sample preparation and with the decrease in total assay time, the MIX·miR sensor can provide results less than an hour after collecting whole blood from a patient presenting with AMI symptoms, less than half the time required to obtain

results from RT-qPCR. This novel approach significantly increases the viability of miRNAs as a biomarker for detection and stratification of AMI, decreasing the time from admission to date-driven clinical intervention.

The results from this study extends the current literature, with all three miRNAs showing a significant increase in concentration during STEMI prior to and following clinical intervention, as well as in patients suffering from CAD (Fig. 5). Additionally, due to its elevated sensitivity, the MIX-miR sensor was able to for the first time provide for the development of a method to non-invasively distinguish between the circumstance of pre-intervention coronary occlusion from that of post-intervention reperfusion through the change in circulating miR-1 and miR-208b expression. This distinction is currently impossible because existing biomarkers used to diagnose AMI are proteins or peptides that require longer time periods to show any discernible change in circulation and have not yet been developed as reliable markers differentiating between occlusion and reperfusion.³ We anticipate that the ability of the MIX-miR sensor to detect differences in miRNA levels within minutes of reperfusion will be of great use to clinicians in guiding patient care, particularly when invasive coronary assessment is not readily available.

Conclusions

The multiplexing capability of MIX-miR, based on its multi-sensor capillary and scalable multisensory board, has allowed us to interrogate a large panel of candidate miRNAs for AMI. In conjunction with the SAW lysing module, this multiplex platform allows us to pinpoint miR-1 to be exosomal and its large but different overexpression for AMI and reperfusion injury suggests that this miRNA, quantified by this platform, can be used to differentiate these two conditions. The ability to quantitatively measure circulating miRNAs in concentrations as low as 1 pM in the original plasma sample with low error can potentially provide a more efficient and accurate measurement than the current biomarkers used clinically while only using a single assay. Additionally, the relative low cost and portability of the developed MIX-miR sensor demonstrates great potential as a rapid, specific miRNA screening tool in both clinical settings and developing countries.

Author contributions

P. Z. and H. C. initiated the ideas and research goals; X. R., B. E., G. R., and C. D. conducted experiments and data collection; X. R. designed, assembled, and tested the PCB; H. C., S. S., P. Z., and X. R. designed and manufactured the MIX-miR sensors; K. M., E. H., C. P., and D. A. collected and prepared patient samples, including NCAD, CAD, STEMI-pre and STEMI-PCI; S. B., S. S., and H. C. provided useful suggestions and assisted the experimental procedures; X. R. and B. E. prepared the manuscript text; B. E., S. S., K. M., C.

P., H. C., and P. Z. edited the manuscript; P. Z. and H. C. provided guidance over the research work.

Conflicts of interest

There are no conflicts to declare.

Acknowledgements

This work is supported by National Institute of Health (NIH) National Heart, Lung, and Blood Institute (NHLBI) under award number R01HL141909 and the Naughton Fellowship. The authors would like to thank Chenguang Zhang and Dr. Zeinab Ramshani from Dr. Hsueh-Chia Chang's group for helpful discussions.

References

- D. J. Hausenloy and D. M. Yellon, *J. Clin. Invest.*, 2013, **123**, 92–100.
- J. Ai, R. Zhang, Y. Li, J. Pu, Y. Lu, J. Jiao, K. Li, B. Yu, Z. Li and R. Wang, *Biochem. Biophys. Res. Commun.*, 2010, **391**, 73–77.
- S. Aydin, K. Ugur, S. Aydin, İ. Sahin and M. Yardim, *Vasc. Health Risk Manage.*, 2019, **15**, 1.
- M. Vafaie, *Diagnosis*, 2016, **3**, 137–142.
- F. Van de Werf, J. Bax, A. Betriu, C. Blomstrom-Lundqvist, F. Crea, V. Falk, G. Filippatos, K. Fox and K. Huber, *Eur. Heart J.*, 2008, **29**, 2909–2945.
- N. C. Chesnaye, K. Szummer, P. Bárány, O. Heimbürger, H. Magin, T. Almquist, F. Uhlin, F. W. Dekker, C. Wanner and K. J. Jager, *J. Am. Heart Assoc.*, 2019, **8**, e013091.
- Z. Wang, X. Luo, Y. Lu and B. Yang, *J. Mol. Med.*, 2008, **86**, 771–783.
- D. A. Chistiakov, A. N. Orekhov and Y. V. Bobryshev, *J. Mol. Cell. Cardiol.*, 2016, **94**, 107–121.
- Y. D'Alessandra, G. Pompilio and M. C. Capogrossi, *Curr. Opin. Cardiol.*, 2012, **27**, 228–235.
- N. Kosaka, H. Iguchi and T. Ochiya, *Cancer Sci.*, 2010, **101**, 2087–2092.
- N. M. Teplyuk, B. Mollenhauer, G. Gabriely, A. Giese, E. Kim, M. Smolsky, R. Y. Kim, M. G. Saria, S. Pastorino and S. Kesari, *Neuro-Oncology*, 2012, **14**, 689–700.
- J. Hayes, P. P. Peruzzi and S. Lawler, *Trends Mol. Med.*, 2014, **20**, 460–469.
- C. Li, F. Pei, X. Zhu, D. D. Duan and C. Zeng, *Clin. Biochem.*, 2012, **45**, 727–732.
- S. De Rosa, S. Fichtlscherer, R. Lehmann, B. Assmus, S. Dimmeler and A. M. Zeiher, *Circulation*, 2011, **124**, 1936–1944.
- L. Zhang, H. Ding, Y. Zhang, Y. Wang, W. Zhu and P. Li, *Front. Physiol.*, 2020, **11**, 1088.
- O. Gidlöf, P. Andersson, J. Van Der Pals, M. Götzberg and D. Erlinge, *Cardiology*, 2011, **118**, 217–226.
- X. Liu, L. Yuan, F. Chen, L. Zhang, X. Chen, C. Yang and Z. Han, *Clin. Lab.*, 2017, **63**, 101–109.

- 18 E. Pinchi, P. Frati, M. Aromatario, L. Cipolloni, M. Fabbri, R. La Russa, A. Maiese, M. Neri, A. Santurro and M. Scopetti, *J. Cell. Mol. Med.*, 2019, **23**, 6005–6016.
- 19 Y. Devaux, M. Mueller, P. Haaf, E. Goretti, R. Twerenbold, J. Zangrandi, M. Vausort, T. Reichlin, K. Wildi and B. Moehring, *J. Intern. Med.*, 2015, **277**, 260–271.
- 20 E. Goretti, M. Vausort, D. R. Wagner and Y. Devaux, *Int. J. Cardiol.*, 2013, **168**, 4548–4550.
- 21 C. Zhang, G. Sun, S. Senapati and H.-C. Chang, *Lab Chip*, 2019, **19**, 3853–3861.
- 22 C. Wang, S. Senapati and H. C. Chang, *Electrophoresis*, 2020, **41**, 1878–1892.
- 23 P. S. Dittrich and A. Manz, *Nat. Rev. Drug Discovery*, 2006, **5**, 210–218.
- 24 X. Ren, P. Ghassemi, Y. M. Kanaan, T. Naab, R. L. Copeland, R. L. Dewitt, I. Kim, J. S. Strobl and M. Agah, *ACS Sens.*, 2018, **3**, 1510–1521.
- 25 X. Ren, P. Ghassemi, J. S. Strobl and M. Agah, *Biomicrofluidics*, 2019, **13**, 044103.
- 26 X. Ren, K. Liu, Q. Zhang, H. M. Noh, E. C. Kumbur, W. W. Yuan, J. G. Zhou and P. L.-G. Chong, *ACS Appl. Mater. Interfaces*, 2014, **6**, 12618–12628.
- 27 P. Ghassemi, K. S. Harris, X. Ren, B. M. Foster, C. D. Langefeld, B. A. Kerr and M. Agah, *Sens. Actuators, B*, 2020, **321**, 128522.
- 28 P. Ghassemi, X. Ren, B. M. Foster, B. A. Kerr and M. Agah, *Biosens. Bioelectron.*, 2020, **150**, 111868.
- 29 Z. Ramshani, F. Fan, A. Wei, M. Romanello-Giroud-Joaquim, C.-H. Gil, M. George, M. C. Yoder, D. Hanjaya-Putra, S. Senapati and H.-C. Chang, *Talanta*, 2021, **225**, 122021.
- 30 Z. Slouka, S. Senapati and H.-C. Chang, *Annu. Rev. Anal. Chem.*, 2014, **7**, 317–335.
- 31 D. Taller, K. Richards, Z. Slouka, S. Senapati, R. Hill, D. B. Go and H.-C. Chang, *Lab Chip*, 2015, **15**, 1656–1666.
- 32 G. Sun, S. Senapati and H.-C. Chang, *Lab Chip*, 2016, **16**, 1171–1177.
- 33 S. Marczak, S. Senapati, Z. Slouka and H.-C. Chang, *Biosens. Bioelectron.*, 2016, **86**, 840–848.
- 34 Z. Slouka, S. Senapati, S. Shah, R. Lawler, Z. Shi, M. S. Stack and H.-C. Chang, *Talanta*, 2015, **145**, 35–42.
- 35 G. Sun, Z. Pan, S. Senapati and H.-C. Chang, *Phys. Rev. Appl.*, 2017, **7**, 064024.
- 36 Z. Yin, Z. Ramshani, J. J. Waggoner, B. A. Pinsky, S. Senapati and H.-C. Chang, *Sens. Actuators, B*, 2020, **310**, 127854.
- 37 S. Sensale, Z. Ramshani, S. Senapati and H.-C. Chang, *J. Phys. Chem. B*, 2021, **125**, 1906–1915.
- 38 Z. Slouka, S. Senapati, Y. Yan and H.-C. Chang, *Langmuir*, 2013, **29**, 8275–8283.
- 39 F. Olivier, R. Antonicelli, M. Lorenzi, Y. D'Alessandra, R. Lazzarini, G. Santini, L. Spazzafumo, R. Lisa, L. La Sala and R. Galeazzi, *Int. J. Cardiol.*, 2013, **167**, 531–536.
- 40 J. Xiao, B. Shen, J. Li, D. Lv, Y. Zhao, F. Wang and J. Xu, *Int. J. Clin. Exp. Med.*, 2014, **7**, 136.
- 41 M. F. Corsten, R. Dennert, S. Jochems, T. Kuznetsova, Y. Devaux, L. Hofstra, D. R. Wagner, J. A. Staessen, S. Heymans and B. Schroen, *Circ.: Cardiovasc. Genet.*, 2010, **3**, 499–506.
- 42 G. Long, F. Wang, Q. Duan, F. Chen, S. Yang, W. Gong, Y. Wang, C. Chen and D. W. Wang, *Int. J. Biol. Sci.*, 2012, **8**, 811.
- 43 C. Li, Z. Fang, T. Jiang, Q. Zhang, C. Liu, C. Zhang and Y. Xiang, *BMC Med. Genomics*, 2013, **6**, 16.
- 44 S. K. Gupta, C. Bang and T. Thum, *Circ.: Cardiovasc. Genet.*, 2010, **3**, 484–488.
- 45 J.-X. Wang, J.-Q. Jiao, Q. Li, B. Long, K. Wang, J.-P. Liu, Y.-R. Li and P.-F. Li, *Nat. Med.*, 2011, **17**, 71–78.
- 46 L.-M. Li, W.-B. Cai, Q. Ye, J.-M. Liu, X. Li and X.-X. Liao, *World J. Emerg. Med.*, 2014, **5**, 182.
- 47 Y.-Q. Li, M.-F. Zhang, H.-Y. Wen, C.-L. Hu, R. Liu, H.-Y. Wei, C.-M. Ai, G. Wang, X.-X. Liao and X. Li, *Clinics*, 2013, **68**, 75–80.
- 48 Y. D'Alessandra, P. Devanna, F. Limana, S. Straino, A. Di Carlo, P. G. Brambilla, M. Rubino, M. C. Carena, L. Spazzafumo and M. De Simone, *Eur. Heart J.*, 2010, **31**, 2765–2773.
- 49 Z. Ramshani, C. Zhang, K. Richards, L. Chen, G. Xu, B. L. Stiles, R. Hill, S. Senapati, D. B. Go and H.-C. Chang, *Commun. Biol.*, 2019, **2**, 189.
- 50 A. S. M. Sayed, K. Xia, T.-L. Yang and J. Peng, *Dis. Markers*, 2013, **35**, 561–566.
- 51 V. Oliveira-Carvalho, V. O. Carvalho and E. A. Bocchi, *DNA Cell Biol.*, 2013, **32**, 8–12.
- 52 E. van Rooij, D. Quiat, B. A. Johnson, L. B. Sutherland, X. Qi, J. A. Richardson, R. J. Kelm Jr and E. N. Olson, *Dev. Cell*, 2009, **17**, 662–673.
- 53 J. T. Shieh, Y. Huang, J. Gilmore and D. Srivastava, *PLoS One*, 2011, **6**, e19481.
- 54 Z. Girmatsion, P. Biliczki, A. Bonauer, G. Wimmer-Greinecker, M. Scherer, A. Moritz, A. Bukowska, A. Goette, S. Nattel and S. H. Hohnloser, *Heart Rhythm*, 2009, **6**, 1802–1809.
- 55 A. H. Wu, Y.-J. Feng, R. Moore, F. S. Apple, P. H. McPherson, K. F. Buechler, G. Bodor and C. C. S. O. C. Standardization, *Clin. Chem.*, 1998, **44**, 1198–1208.
- 56 X. Ji, R. Takahashi, Y. Hiura, G. Hirokawa, Y. Fukushima and N. Iwai, *Clin. Chem.*, 2009, **55**, 1944–1949.
- 57 N. N. S. B. Nik Mohamed Kamal and W. N. S. Shahidan, *Front. Pharmacol.*, 2019, **10**, 1500.